Chapter-3

In Vivo Characterization of Luffa-based Composite Scaffolds upon Subcutaneous Implantation in Rats

3.1 Introduction

The human body is susceptible to tissue and organ damage caused by a diverse range of pathologies, encompassing ailments such as congenital anomalies, traumas, cancer, and injuries. Applications of tissue engineering often involve using three-dimensional (3D) scaffolds to provide an appropriate microenvironment for the inclusion of cells or growth factors to regenerate damaged tissues or organs. The scaffolds aim to mimic the actual microenvironment that exists in vivo, where cells interact and respond in response to the mechanical signals they acquire from their surrounding three-dimensional environment (Ikada 2006; Mao and Mooney 2015; Hosseinkhani et al. 2014).

Luffa cylindrica (LC), a naturally derived plant-based material, has been extensively studied and demonstrated to possess excellent biocompatibility properties. As a scaffold material, it exhibits remarkable inertness within the host organism, eliciting minimal immune reactions or adverse responses, making it a highly suitable candidate for tissue engineering applications. Its interconnected pores facilitate effective cell infiltration, nutrient diffusion, and waste removal. This intricate porous architecture closely resembles the native extracellular matrix (ECM) of tissues; promoting cell adhesion, migration and successful tissue regeneration. The mechanical strength and stiffness of luffa-based scaffolds can be tailored to accommodate various tissue engineering needs; providing flexibility in design and application (Mohapatra and Rautray 2021; Gundu et al. 2022). Moreover, luffa scaffolds can be functionalized to incorporate growth factors and bioactive molecules, which play a pivotal role in promoting cell proliferation, differentiation and tissue regeneration. This unique ability to deliver bioactive factors significantly enhances the scaffold's regenerative potential and therapeutic efficacy (Patamia et al. 2022). On the other hand, gelatin, with its inherent cell-binding domains such as the RGD sequence, exhibits exceptional cell adhesion, spreading and proliferation properties. This characteristic enables robust cell attachment to the scaffold, fostering the

population and growth of cells within the structure. As a result, gelatin-based scaffolds offer a conducive environment for cellular activities and hold great promise for various engineered tissue applications (A. Y. Kim et al. 2017; Afewerki et al. 2019).

Currently, subcutaneous implantation in small animal models is widely employed, aiming to evaluate immune response and tissue regeneration. Among these, subcutaneous implants in the small animal models (e.g., rats) have become one of the most extensively studied approaches, primarily due to their ability to facilitate the comprehensive assessment of tissue compatibility, including systemic toxicity, implantation effects, histological analysis, carcinogenicity, biodegradation, and immune response (Khorramirouz et al. 2018; Liu et al. 2018). Quantification of the biocompatibility of an implant can be achieved through the assessment of blood parameters after implantation. The investigation entails the acquisition of blood samples both prior to and after implantation, followed by a comprehensive analysis of the variations in various blood constituents. Quantification of blood parameters after implantation holds significant potential in the early detection of potential complications associated with the implant (Divakar et al. 2020). The implementation of preventive measures has been shown to effectively mitigate the occurrence of severe complications, including infection or rejection. Moreover, through quantification of blood parameters researchers and healthcare professionals can gain valuable insights into the performance and functionality of implants (Zawidlak-Węgrzyńska et al. 2022).

In the previously reported work, we successfully fabricated luffa-based composite scaffolds using the freeze-drying technique and performed invitro characterizations of the scaffolds (Gundu et al. 2022). The scaffolds were found favorable for cellular compatibility (MG-63 osteoblast-like cells) and exhibited excellent adherence and proliferation within the scaffolds, and retained significantly higher viability even after 5 days of culture (Gundu et al. 2022). In

this chapter, we extended our previous findings by examining the biocompatibility of the luffa-based scaffolds in a subcutaneous in vivo rat model. We divided the 3% LC, 5% LC, control scaffolds, and Sham into groups and performed histopathological investigation and biochemical quantification to assess the biocompatibility of the implants under in vivo conditions. The scaffolds were subcutaneously implanted in Wistar rats and assessed their integration with the host tissue. Histological investigations of implanted scaffolds and various organs, including the heart, liver and kidney, have been examined, and further biochemical characterizations such as aspartate transaminase (AST) /alkaline phosphatase(ALP) /alanine transaminase (ALT) and bilirubin levels of the liver, serum creatinine of the kidney, and creatine phosphokinase-MB (CK-MB) of the heart were performed.

3.2 Materials and Method

3.2.1 Materials

The 4% paraformaldehyde, nutrient broth, AgarAgar Type 1, and ampicillin were purchased from HiMedia, India. The aspartate aminotransferases (AST)-modified IFCC (International Federation of Clinical Chemistry) kits, alanine aminotransferases (ALT)-modified IFCC kits, creatine phosphokinase-MB (CK-MB) serum creatinine assay kits, and bilirubin assay kits, assay kits were obtained from TARA clinical Systems, India. The materials utilized for the chemical treatment of LC and biomaterials used for the fabrication of scaffolds were discussed in our previously published article (Gundu et al. 2022). The bacterial strains Escherichia coli (BCRC11634) were obtained from the Department of Microbiology, Osmania University, Hyderabad.

3.2.2 Fabrication of composite scaffold

The fabrication of porous composite scaffolds with 3% LC, 5% LC, and the control (C) was accomplished through the freeze-drying process using LC, Gelatin, Hydroxyapatite, and Psyllium husk, as detailed in our research article (Gundu et al., 2022). A 10% gelatin (G) solution was stirred on a hot plate at 200 rpm and 40°C for 30 min. Subsequently, 1% HA was added to the gelatin solution, and continuous stirring ensured a homogeneous mixture. Following this, 3% LC powder was introduced into the gelatin solution, and stirring persisted for 2 h until the powder was evenly dispersed throughout the solution. The gelatin solution was then combined with 2.5% psyllium husk (PH) powder and vigorously mixed until a stable viscosity. The same method was employed to create both the 5% LC scaffold and the control (C), without LC powder. Moreover, glutaraldehyde was utilized for cross-linking the molecules to enhance their structural integrity. To ensure the suitability of the prepared scaffolds (3% LC, 5% LC, and control (C)) for implantation, a thorough sterilization process involving 70% ethanol treatment was carried out. Subsequently, exposure to UV light was performed to ensure complete sterilization and to maintain aseptic conditions.

3.2.3 Ethical approval

The fabricated composite porous scaffolds were evaluated for biochemical analysis using a Wistar rat model. The research strictly followed the guidelines stipulated by the committee for control and supervision of experiments carried out on animals (CPCSEA). Ethical approval for the study was granted by the Central Animal Ethical Committee at the Institute of Medical Science, at Banaras Hindu University, Varanasi, on March 3, 2022 (IAEC approval number: IIT(BHU)/IAEC/2022/071. For the investigation, adult Wistar rats weighing 150-230 g each were carefully selected and were acclimatized for a week under specific conditions. The environmental conditions were maintained at a natural light/dark cycle with a temperature maintained at 25 ± 2°C and a humidity level of 55-60%. Additionally, an appropriate rodent

pellet diet and water *ad libitum* were provided to ensure their well-being during the adaptation period.

3.2.4 Animals grouping for scaffold implantation

In accordance with the authorized guidelines, a cohort of twelve male Wistar rats, weighing between 150-220 g was used for the experiment. These rats were divided into four distinct groups: Group A (3% LC), Group B (5% LC), Group C (Control), and Group D (Sham). Each group consisted of three rats, resulting in a total sample size of n=3. Prior to the procedures, the rats were administered intraperitoneal doses of ketamine (35 mg/kg) and xylazine (5-10 mg/kg) to induce sedation. The dorsal area of each rat was prepared by trimming the hair and cleansing the skin surface with 70% ethanol solution. Subsequently, a circular incision with an approximate diameter of 12 mm was carefully created, and the respective fabricated scaffolds from each group were subcutaneously implanted in the dorsal region of the rats. To investigate potential indications of systemic inflammatory response, an extensive analysis of serum biochemistry was performed. Upon euthanasia, ~ 2 mL of blood was extracted through cardiac puncture and carefully stored in serum coagulation vials to ensure optimal conditions for biochemical investigations. The serum biochemistry parameters subjected to thorough investigations including creatine phosphokinase-MB (CK-MB), serum creatinine, alkaline phosphatase (ALP), alanine transaminase (ALT), aspartate aminotransferase (AST), and bilirubin were assessed to determine the functionality of the heart, kidneys and liver, respectively. The blood samples were analyzed by Dr. Lal Pathlabs laboratory, New Delhi, India.

3.2.5 Histopathological studies

After a period of 21 days, the implanted rats were euthanized, and the scaffolds along with associated tissue and organs such as the liver, heart, and kidneys were isolated from their bodies and preserved in a 4% formalin solution for tissue fixation. Sequential dehydration and sectioning of the samples were performed, followed by infiltration of molten paraffin. Tissue blocks were then generated by embedding the paraffin-permeated samples into moulds containing paraffin. The blocks were sliced into thin sections of thickness of ~5 μm using a microtome machine and later stained with hematoxylin and eosin (H&E) for histopathological investigation to visualize the tissue structure and cell morphology. The prepared stained slides were examined under an upright bright-field high-resolution microscope (OLYMPUS) and the images were captured using the To up View 3.7 software.

3.2.6 Biochemical analysis of serum

Performing biochemical analysis by collecting blood samples before and after the implantation process is crucial to facilitate a comprehensive investigation of the implanted scaffolds in rats. By comparing the pre-and post-implantation blood samples, it is feasible to evaluate abnormalities in specific biochemical parameters, including creatine phosphokinase-MB (CK-MB), serum creatinine, alkaline phosphatase (ALP), alanine transaminase (ALT), aspartate aminotransferase (AST) and bilirubin. These investigations provide valuable insights into the enzymatic activities of the heart, kidney, and liver by allowing comparisons between the control and experimental groups. The enzyme activities were assessed using commercially available kits.

3.2.6.1 CK-MB

The CK-MB (Creatine Kinase-MB) test is a hematological assay used to assess the extent of myocardial injury, particularly in cases of myocardial infarction. The enzymatic protein creatine kinase is primarily found in skeletal muscle and cardiac tissue. By quantifying the concentration of this specific enzyme in the bloodstream, the CK-MB assay provides valuable information about the potential damage to the cardiac muscle. This investigation serves as an essential tool for evaluating the presence and severity of myocardial damage in terms of heart-related conditions.

3.2.6.2 Serum creatinine

Performing a serum creatinine test determines the amount of creatinine present in the blood. The regular metabolism of muscle results in the production of a waste product known as creatinine, which is then filtered by the kidneys before being expelled from the body into the urine. The measurement of serum creatinine is a fundamental marker for evaluating kidney health and detecting diseases that are associated with renal function. The impaired kidney function may not effectively filter creatinine, resulting in elevated serum creatinine levels. High serum creatinine levels may suggest decreased kidney function, and it can be an early sign of kidney disease/damage. Determining the amount of creatinine that is present in the bloodstream involves collecting a blood sample from a rat and analyzing it in the laboratory. The results are reported in milligrams per deciliter (mg/dL) unit of measurement.

3.2.6.3 Assessment of liver function (AST/ALP/AST and bilirubin levels)

The blood tests, including those to detect bilirubin levels and specific liver enzymes, are conducted to evaluate liver function assess the overall health and performance of the liver and to identify any potential liver issues or diseases. Both aspartate aminotransferase (AST) and alanine aminotransferase (ALT) are known as aminotransferases, with the majority of these

enzymes located within liver cells. An elevation in AST and ALT levels in the blood may indicate the presence of liver cell injury or damage. Alkaline phosphatase (ALP) is an enzyme found in various organs, including the liver and bones. The normal range of ALP is 30 to 130 IU/L, while AST level ranges from 50 to 150 IU/L and ALT are typically between 10 to 40 IU/L - 44 to 147 IU/L. The elevated levels of alkaline phosphatase (ALP) are often associated with conditions affecting the liver and bones (Hasan, Tamanna, and Haque 2018).

Bilirubin is a yellow pigment formed when the hemoglobin in red blood cells breaks down. The liver is responsible for breaking down bilirubin, and the waste is excreted into the bile. Abnormally high levels of bilirubin in the blood may suggest liver dysfunction or blocked bile ducts. These blood tests are valuable in assessing liver health and detecting potential liver-related problems or diseases. Proper interpretation of the results, along with other clinical information, is crucial in understanding liver conditions and determining appropriate management if any issues are identified.

3.2.7 Antibacterial sustained drug release from fabricated scaffolds

The antibacterial test evaluated the drug release capacity of the fabricated scaffolds using a disc diffusion test against gram-negative Escherichia coli (E.coli). The pathogen colonies were picked with a wire loop and introduced into a test tube containing the nutrient media to facilitate bacterial growth. A mixture of the nutrient and agar medium was then added to the sterilized Petri plates following which they were incubated for 24 h in an incubator. For analysis of the bactericidal sustained release effect from the scaffolds, 0.l mL of the inoculated pathogens were uniformly cultured over Petri plates containing an agar medium using the spread plate technique. The fabricated scaffolds, including 3% LC, 5% LC, control (C), and Whatman filter paper (positive control), were cut into disc shapes and sterilized in 70% ethanol for 24 h, followed by 30 min of ultraviolet radiation before the studies. The sterilized scaffolds and

control disc were soaked in 1 mg/mL ampicillin solution for 15 min and subsequently placed on agar plates and incubated for 24 h at 37°C. The area of inhibition zones was captured using a digital camera to analyze the bactericidal effect of the samples after 24 h.

3.3 Statistical analysis

The experiments were repeated three times, and the results were presented as the mean value along with the standard deviation. For statistical analysis, all experimental data underwent ANOVA, followed by Tukey's multiple comparison tests. The graphs were plotted using OriginPro 2020 software (OriginLab).

3.4 Results and Discussion

3.4.1 Histopathological analysis of scaffolds implanted

The histological analysis revealed that the implanted scaffolds remained securely at the site of implantation throughout the study duration. The results indicated that surgical implantation of luffa-based scaffolds i.e. 3% LC, 5% LC, and control scaffolds in rats had shown no adverse effects compared to Sham (positive control) (Figure 3.1). Figure 3.1 illustrates the structural integrity of the 3% LC and 5% LC scaffolds and demonstrates excellent compatibility with the surrounding tissues exhibiting well-defined pores within the scaffold, attributed to the inclusion of luffa. This probably enhances the scaffold’s ability to resist degradation and maintain its structural integrity. The porous architecture of the scaffold plays an essential function in facilitating vascular growth and promoting cell proliferation. The control scaffold (without luffa), also demonstrates biocompatibility with the gradual deterioration of porous architecture compared to luffa-containing scaffolds 3% and 5% LC. The study shows that the scaffolds demonstrated excellent biocompatibility and stability, ensuring their suitability for potential applications in tissue engineering and regenerative medicine.

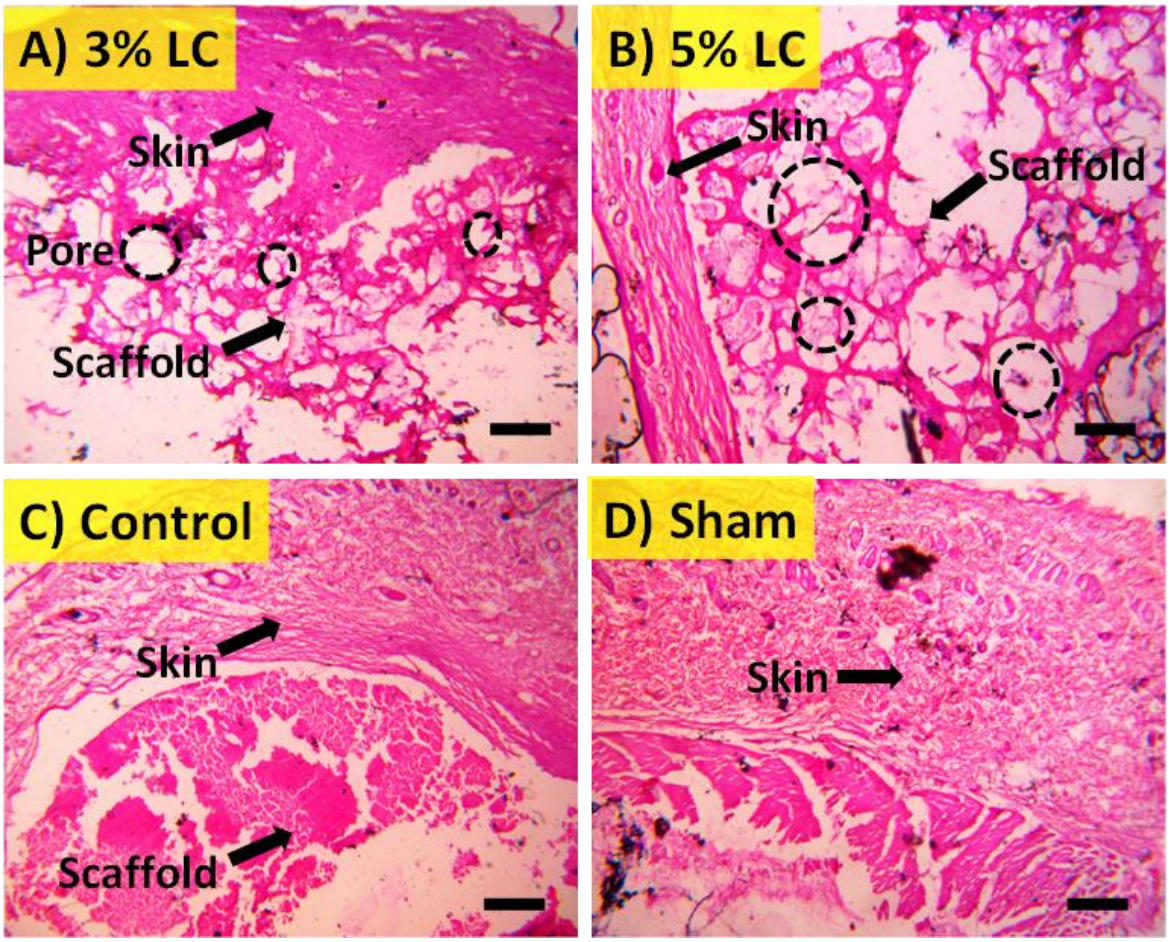

Figure 3.1: Histological images of luffa-based scaffolds A) 3% LC, B) 5% LC, C) Control scaffold (without LC), and D) Sham (positive control) harvested after 3 weeks of implantation in Wistar rat model, subcutaneously. The figure illustrates the scaffold morphology and presence of pores in vivo. Scale bar: 100 µm.

3.4.2 Histopathological analysis of organs of rats implanted with scaffolds

3.4.2.1 Heart (CK-MB)

The histological examination of heart tissue through light microscopy provided clear evidence of the excellent biocompatibility of the scaffolds in all the experimental groups (3% LC, 5% LC, and control) and the control group (Sham). Figure 3.2 clearly illustrates the presence of a well-organized network of cardiac muscle fibers, representing normal myocardium. These cardiac muscle fibers exhibit a distinct striated pattern and are interconnected, forming a highly coordinated and functional structure. Notably, the arrangement of muscle fibers can be easily observed, and the presence of intercalated discs between adjacent muscle cells is evident, facilitating rapid electrical communication between cells. There were no signs of inflammation,

fibrosis, or any other pathological alterations observed in the heart tissue samples, indicating the absence of adverse effects on the myocardium. Prominently, there was no evidence of an acute inflammatory response after implantation. As the implantation progressed, the blood vessels started to infiltrate the scaffold, leading to the formation of neovascularization. This process provided a vital supply of oxygen and nutrients to the implanted scaffold, thereby promoting the survival and growth of cells within the scaffold. The absence of detrimental impacts on the myocardium and the presence of normal tissue architecture and function confirms the excellent biocompatibility of the implanted scaffolds. The results obtained from this histological examination reinforce the suitability of the scaffolds for potential applications in tissue engineering and regenerative medicine, as they have demonstrated their ability to integrate well with the surrounding tissue and support favorable tissue responses.

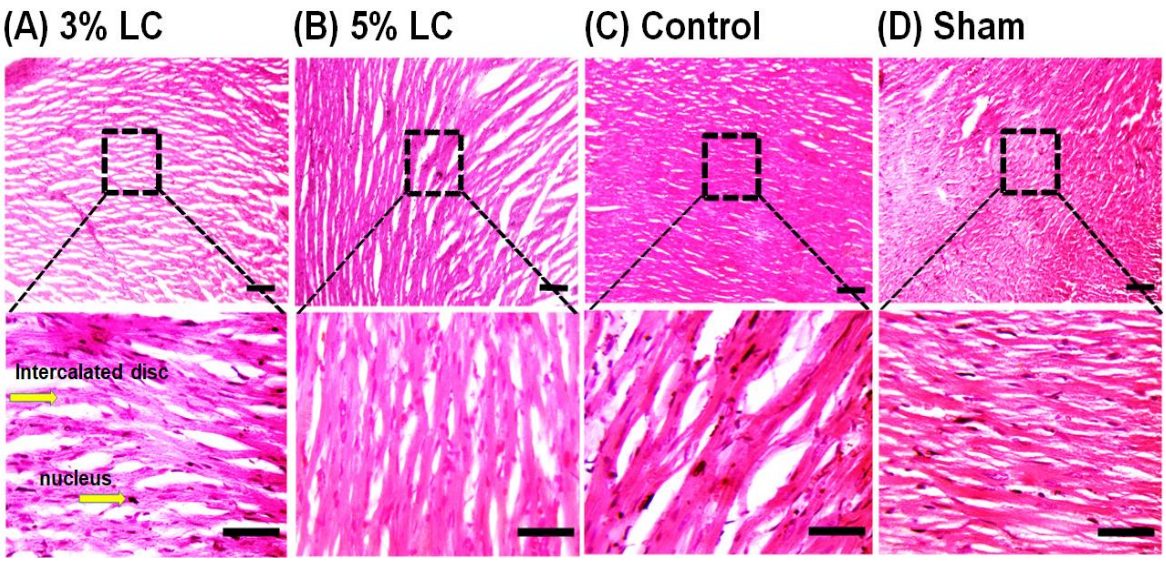

Figure 3.2: H&E staining of pathological sections of heart tissues after 3 weeks implantation of scaffold: A) 3% LC, B) 5% LC, C) control (without LC), and D) Sham (positive control). The figure depicts clear evidence of the excellent biocompatibility of the scaffolds. Scale bar: 100 µm.

3.4.2.2 Kidney (Serum creatinine)

Biocompatibility assessment was carried out by subcutaneously implanting scaffolds in rats for a duration of 3 weeks. The study findings demonstrated that the implanted scaffolds had no

adverse impact on the kidney tissues. Furthermore, the histological structure of the kidney in all experimental groups closely resembled that of the control group (Sham) as depicted in Figure 3.3. In addition, no indications of inflammatory reactions, organ toxicity, or systemic toxicity were observed in any of the experimental groups, which reaffirmed the excellent biocompatibility of the implanted scaffolds. In the histological images, an intriguing observation was the visualization of Bowman's space, which appeared to open into the beginning of a proximal tubule at the urinary pole. However, due to the thick sections of the specimens, it can be difficult to properly establish the particular identities of cells that make up the glomerulus (endothelial cells, podocytes, or mesangial cells) and therefore found very challenging to reliably determine.

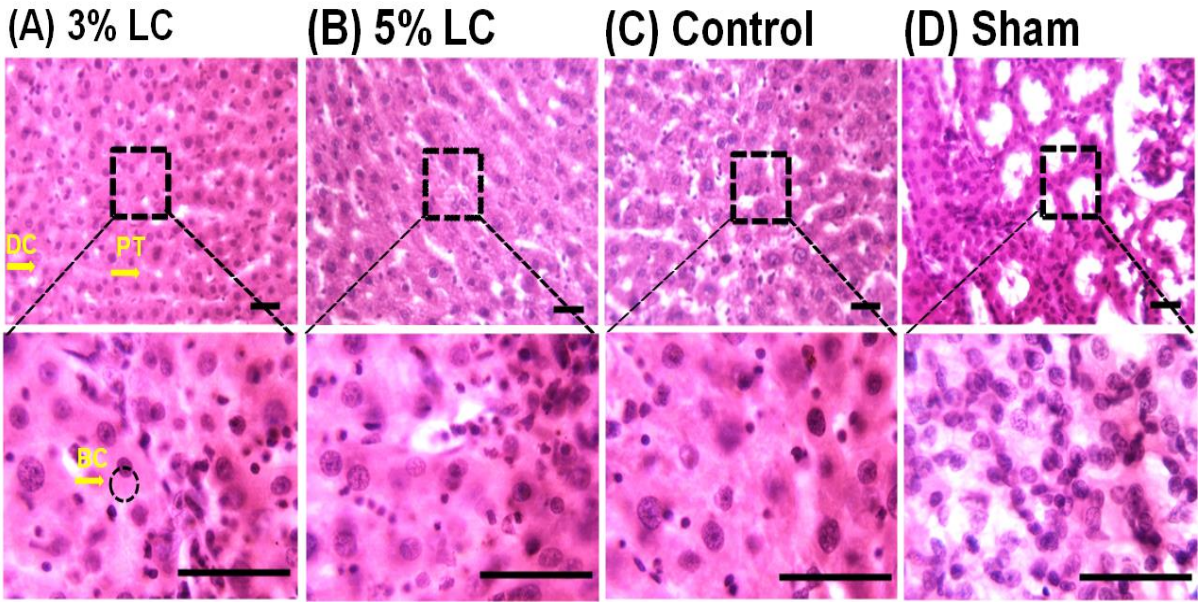

Figure 3.3: Histological examination of kidney tissues demonstrated that the implanted scaffolds had no adverse impact on the kidney tissues for the implanted scaffolds (i.e., 3% LC, 5% LC, and control compared to the control group (Sham)). Scale bar: 100 µm.

3.4.2.3 Liver

The histological examination, along with liver enzyme evaluations, offers compelling evidence supporting the excellent biocompatibility of the implanted scaffold in the liver. Notably, the results revealed no significant differences between the groups with the implanted scaffolds and the Sham group. These findings strongly suggest that the scaffold's presence did not trigger any adverse effects on the liver tissues (Figure 3.4).

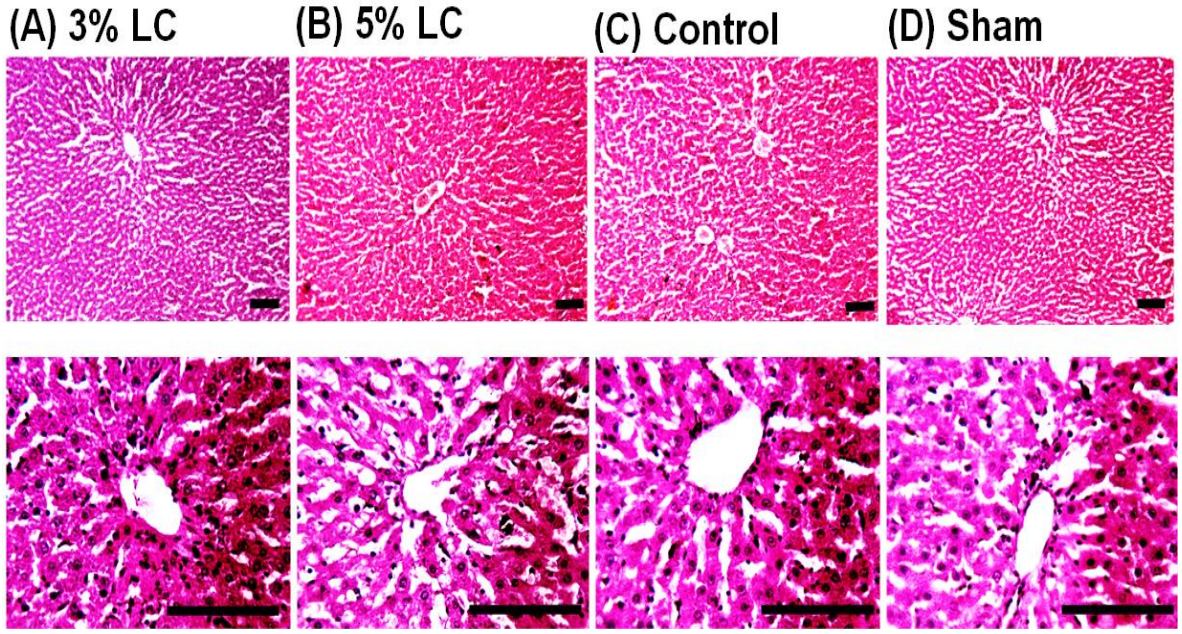

Figure 3.4: Histological examination of liver tissues demonstrated that the implanted scaffolds had no adverse impact on the liver tissues for the implanted scaffolds (i.e., 3% LC, 5% LC, and control compared to the control group (Sham)).

3.4.3 Biochemical analysis

3.4.3.1 CK-MB

CK-MB is a crucial cardiac biomarker, commonly employed to assist in diagnosing myocardial infarction. Detecting CK-MB in the bloodstream holds crucial diagnostic significance for identifying myocardial infarction (Modulevsky, Cuerrier, and Pelling 2016; Natsukawa et al. 2017). CK is an enzyme composed of dimers, catalyzing the reversible phosphorylation of

creatine by ATP, resulting in the production of phosphor creatine and ADP (Kurapati and Soos 2023). Typically, CK-MB isoenzymes constitute about 15% of the myocardium and 1-3% of skeletal muscles, respectively. In the myocardium, 15% of CK is in the form of CK-MB, while the remaining 85% is CK-MM found in skeletal muscles (Kurapati and Soos 2023). Although CK-MB is present in small amounts in other tissues, the myocardium has the highest proportion of CK-MB compared to others. Serum CK-MB of human myocardium reference values normally range from 3 to 5 or 5 to 25 IU/L (Cabaniss 1990; Hasan, Tamanna, and Haque 2018; Kurapati and Soos 2023; Yilmaz et al. 2006; G Srikanth et al. 2009). Therefore, when there is a rapid and significant release of CK-MB into the blood, it suggests damage to the heart muscle, which largely indicates acute myocardial infarction (Ota et al. 2020). Elevated levels of creatine phosphokinase MB (CK-MB) are considered biochemical markers of myocyte necrosis (Yilmaz et al. 2006). Figure 3.5 illustrates the serum concentration of CK-MB across four distinct groups: 3% LC, 5% LC, Control, and Sham (control group) during the initial phase (24 h) of investigation. The measured CK-MB levels were determined as 38.75 ± 1.45 U/L for the 3% LC group, 38.35 ± 5.29 U/L for the 5% LC group, 30.53 ± 5.35 U/L for the Control group, and 17.25 ± 3.88 U/L for the Sham group. Furthermore, after three weeks of implantation, the values of the various scaffolds (3% LC, 5% LC, control, and sham) are 22.35 ± 4.25 U/L, 23.75 ± 5.51 U/L, 20.53 ± 6.35 U/L and 15.25 ± 4.24 U/L, respectively. To assess the changes in serum CK-MB levels among these groups, a one-way ANOVA analysis was performed. The results of the analysis revealed significant differences in serum CK-MB concentration between all three groups (3% LC, 5% LC, and Control) when compared to the Sham (control) group during the initial days (24 h) of the study (Cabaniss 1990). Remarkably, despite these differences, CK-MB levels in all groups remained within the range of standard reference values. As the study progressed over subsequent weeks, it was observed that the CK-MB levels

in all groups exhibited a gradual reduction, eventually returning to the normal range after three weeks of observation exhibiting no significant difference with respect to the Sham group.

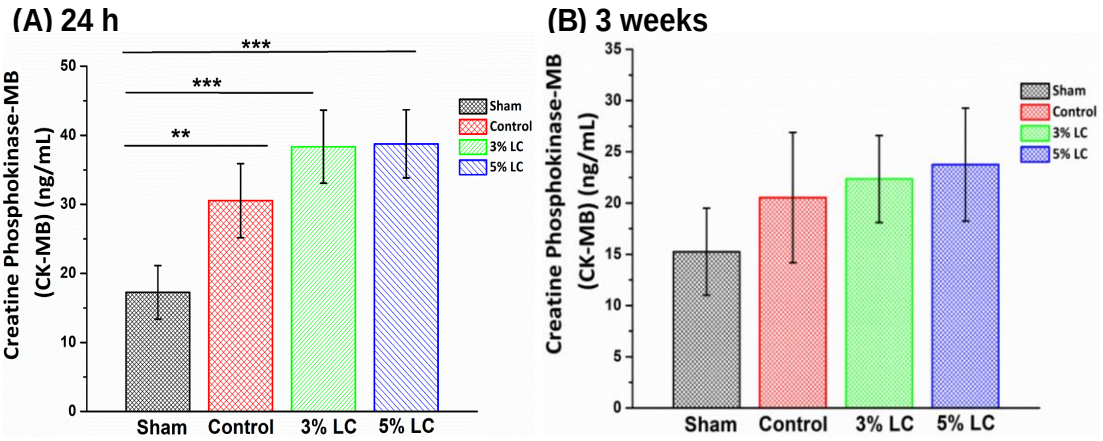

Figure 3.5: The plot illustrates the biochemical values of creatinine phosphokinase-MB (CK-MB) of the experimental group in comparison to the control group. Figure A depicts the values after 24 hours post-implantation, while Figure B displays the values after three weeks of implantation.

3.4.3.2 Serum creatinine

The kidneys are essential for maintaining the equilibrium of creatinine levels in the bloodstream through effective filtration and excretion in the urine. The typical reference range for serum creatinine in humans is between 0.63 to 1.16 mg/dL (Delanaye, Cavalier, and Pottel 2017) and in rats is 0.4 to 0.8 mg/dL (Thammitiyagodage et al. 2020), and under normal conditions, creatinine levels in the blood remain relatively consistent. However, elevated creatinine levels may indicate compromised kidney function, which could be a sign of kidney disease. The difficulty in filtering creatinine can result in an accumulation of creatinine in the blood. Figure 3.6 presents the findings regarding creatinine levels across different groups. Specifically, figure 3.6 (A) displays values obtained 24 hours after implantation for 3% LC, 5% LC, control scaffolds, and the Sham group, revealing creatinine levels of 1.25 ± 0.20 mg/dL, 1.37 ± 0.33 mg/dL, 1.02 ± 0.28 mg/dL, and 0.78 ± 0.10 mg/dL, respectively. Additionally, the subsequent creatinine values after 3 weeks are as follows: 1.10 ± 0.23 mg/dL,

1.13 ± 0.29 mg/dL, 1.01 ± 0.30 mg/dL, and 0.82 ± 0.25 mg/dL for 3% LC, 5% LC, control, and Sham groups (depicted in figure 3.6 B).

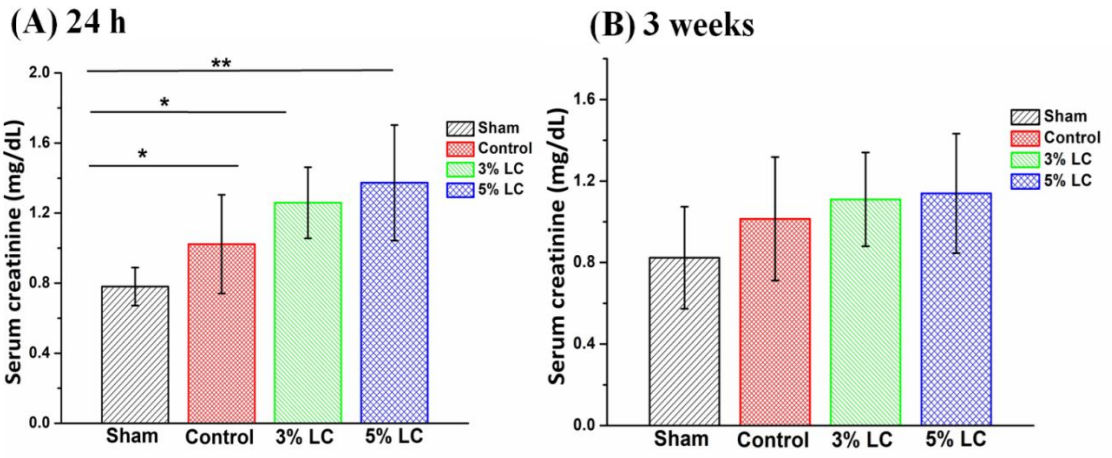

Figure 3.6: The figure depicts the serum creatinine's biochemical values. Graph A shows the values 24 hours after implantation, and Graph B exhibits the values after three weeks of implantation.

3.4.3.3 AST/ALP/ALT and bilirubin levels

The levels of AST, ALT, and ALP serve as crucial enzyme biomarkers utilized to monitor liver structural integrity and to detect potential liver toxicity conditions. However, elevated levels of serum aminotransferases have also been associated with a number of other medical conditions, including dementia, stroke, colorectal adenoma, frailty, disability, sarcopenia, metabolic syndrome (MS), and liver injury. It is important to note that elevated serum aminotransferases do not always indicate liver damage. In some cases, elevated levels of these enzymes may be due to other factors, such as muscle damage, heart disease, or certain medications (Chinnappan et al. 2023; H. Kim and Han 2018). Therefore, we have measured serum aminotransferase levels before and after implantation of the scaffold.

The assessment of the impact of luffa-based scaffold implantation in rats involved the examination of serum levels of these enzymes at two-time points: 24 hours (Figure 3.7) and after 3 weeks (Figure 3.8). In cases of organ injury or damage, such as during scaffold

implantation, these enzymes can be released into the bloodstream. Therefore, the levels of AST, ALT, and ALP in the rat serum were carefully examined to determine any potential effects of the luffa-based scaffold on liver function.

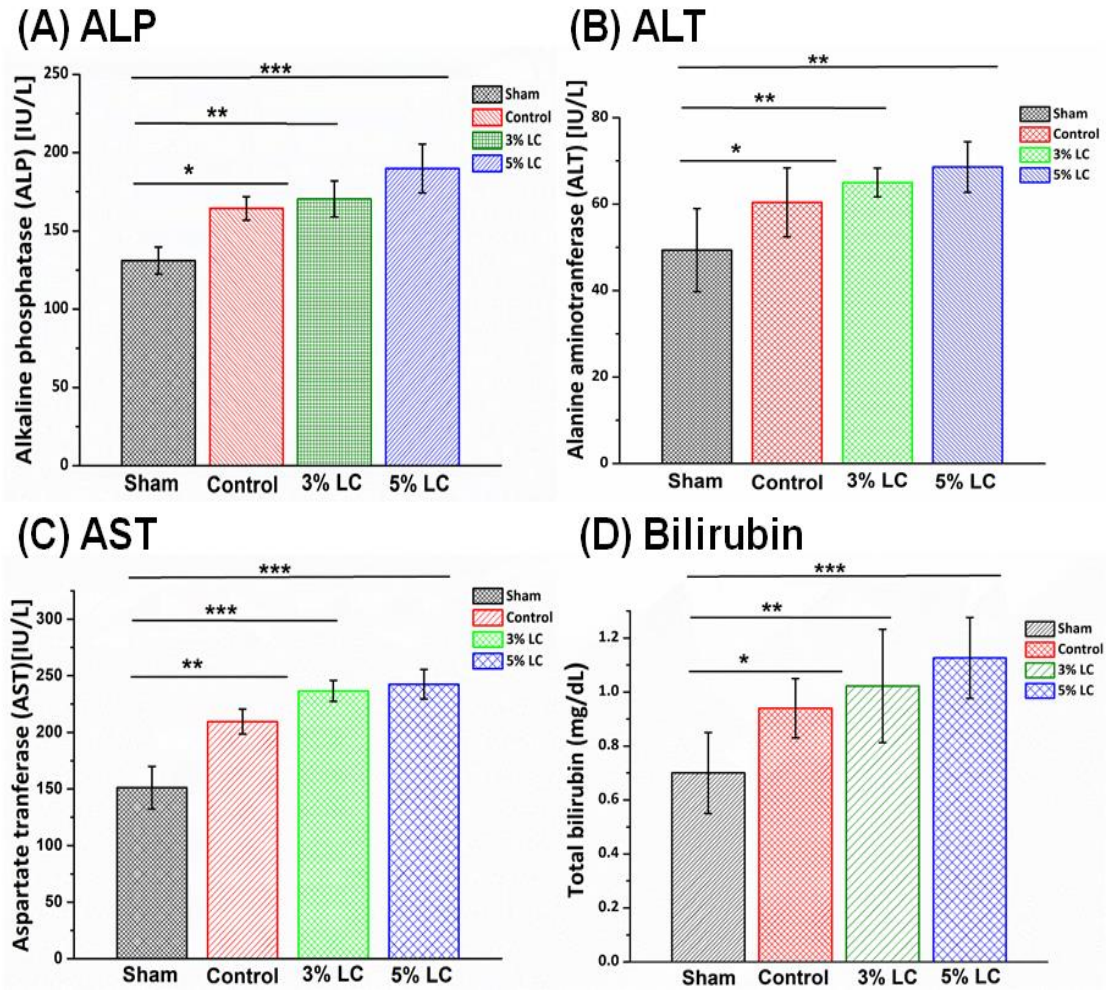

Figure 3.7: The figure depicts the values of A) ALP, B) ALT, C) AST, and D) bilirubin of various experimental groups compared to the control group (Sham) after 24 h of scaffold implantation in rats.

The reference ranges for AST, ALT, and ALP are 50 to 150 U/L, 10 to 40 U/L, and 30 to 130 U/L, respectively (Hasan, Tamanna, and Haque 2018) provided benchmarks for evaluating liver enzyme levels in the experimental groups. The study outcomes revealed that in the control group (Sham), the AST levels after 24 h were 151.23 ± 18.67 U/L, whereas in the experimental

groups 3% LC, 5% LC, and control, the AST levels were 236.7 ± 9.21 U/L, 242.6 ± 12.87 U/L, 209.6 ± 10.97 U/L, respectively. After 3 weeks, the biochemical values for 3% LC, 5% LC, control, and Sham were 156.7 ± 8.25 U/L, 169.6 ± 12.56 U/L, 146 ± 10.74 U/L, and 140.23 ± 12.67 U/L, respectively. Similarly, the ALT levels after 24 h in the 3% LC, 5% LC, control, and Sham groups were 65.0 ± 3.31 U/L, 68.65 ± 5.85 U/L, 60.4 ± 7.98 U/L, 49.36 ± 9.60 U/L, respectively. After 3 weeks, the corresponding values were 63.6 ± 5.85 U/L, 60 ± 3.316 U/L, 52.4 ± 7.98 U/L, and 48.36 ± 10.60 U/L for 3% LC, 5% LC, control and Sham, respectively. Furthermore, the ALP levels at 24 h and after 3 weeks were as follows: 3% LC (170.4 ± 11.50 U/L, 151.4 ± 11.5 U/L), 5% LC (189.8 ± 15.55 U/L, 169.8 ± 9.55 U/L), control (164.4 ± 7.5 U/L, 134.4 ± 7.5 U/L), and Sham (131.5 ± 8.58 U/L, 130.05 ± 8.58 U/L). The bilirubin levels for 3% LC, 5% LC, control, and sham after 24 h were 1.02 ± 0.21 U/L, 1.12 ± 0.15 U/L, 0.15 ± 0.94 U/L and 0.7 ± 0.15 U/L, respectively. After three weeks, the corresponding values were 0.90 ± 0.11 U/L, 0.91 ± 0.10 U/L, 0.80 ± 0.08 U/L and 0.7 ± 0.15 U/L for 3% LC, 5% LC, control, and sham, respectively.

Interestingly, the results indicated that the implantation of the luffa-based scaffold in rats resulted in varying degrees of changes in liver enzymes, particularly when compared to the Sham group. However, it is important to note that the significant elevation in AST, ALT, and ALP levels observed in the experimental groups did not indicate any potential adverse effects on liver function or cellular integrity. This conclusion is drawn from the fact that the serum levels of these enzymes in the scaffold-implanted groups remained within the range of normal reference values. As a result, the study findings suggested that the implanted scaffolds did not induce any toxicity at the implantation site. Additionally, the bilirubin levels in all the scaffold-implanted groups did not show any significant difference when compared to the Sham group. This further supported the concept that the luffa-based scaffold implantation did not lead to any adverse effects on liver function or bilirubin metabolism. Table 3.1 represents a

comprehensive overview of the biochemical values associated with the different types of scaffolds.

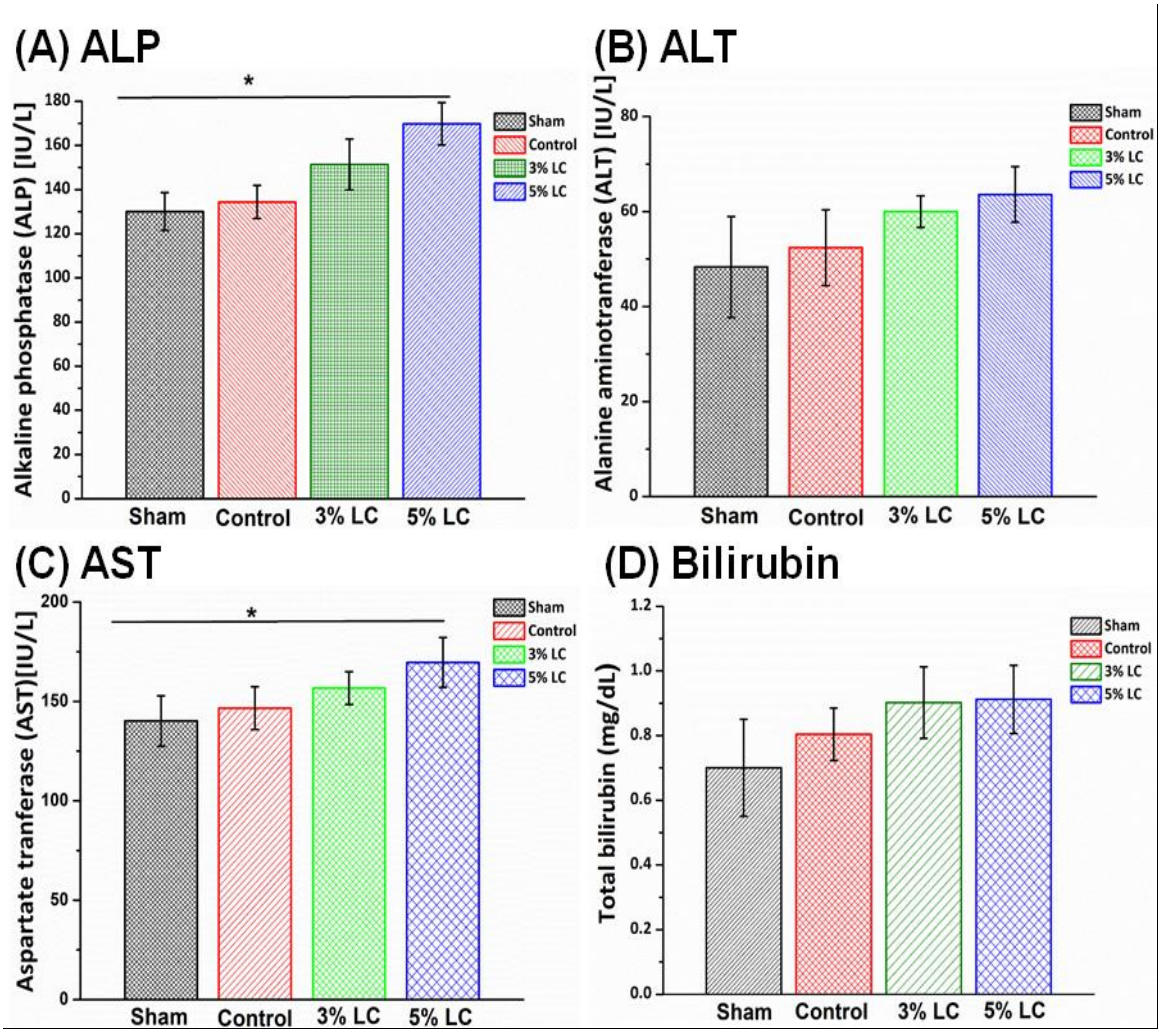

Figure 3.8: The figure depicts the values of A) ALP B) ALT C) AST and D) bilirubin of various experimental groups compared to the control group (Sham) after 3 weeks of scaffold implantation in rats.

Table 3.1: Depicts the biochemical parameters of the heart, kidney, and liver of rats implanted with various scaffolds.

Biochemical Parameters	3% LC	5% LC	Control (C)	Sham
AST (U/L), 24 h	236.7 ± 9.21	242.6 ± 12.87	209.6 ± 10.97	151.23 ± 18.67
AST (U/L), 3 weeks	156.7 ± 8.25	169.6 ± 12.56	146 ± 10.74	140.23 ± 12.67
ALT (U/L), 24 h	65 ± 3.31	68.6 ± 5.85	60.4 ± 7.98	49.36 ± 9.60
ALT (U/L), 3 weeks	63.6 ± 5.85	60 ± 3.316	52.4 ± 7.98	48.36 ± 10.60
ALP(U/L), 24 h	170.4 ± 11.5	189.8 ± 15.55	164.4 ± 7.5	131.05 ± 8.58
ALP(U/L), 3 weeks	151.4 ± 11.5	169.8 ± 9.55	134.4 ± 7.5	130.05 ± 8.58
Bilirubin total (mg/dL), 24 h	1.02 ± 0.21	1.12 ± 0.15	0.15 ± 0.94	0.7 ± 0.15
Bilirubin total (mg/dL), 3 weeks	0.90 ± 0.11	0.91 ± 0.10	0.80 ± 0.08	0.7 ± 0.15
Serum Creatinine (mg/dL), 24 h	1.58 ± 0.20	1.69 ± 0.37	1.34 ± 0.32	1.10 ± 0.10
Serum Creatinine (mg/dL), 3 weeks	1.49 ± 0.30	1.59 ± 0.30	1.34 ± 0.33	1.02 ± 0.30
CPK-MB (U/L), 24 h	38.75 ± 4.93	38.35 ± 5.29	30.53 ± 5.35	17.25 ± 3.88
CPK-MB (U/L), 3 weeks	22.35 ± 4.25	23.75 ± 5.51	20.53 ± 6.35	15.25 ± 4.24

3.4.4 Antibacterial drug release on fabricated scaffolds

The drug release behavior was assessed by examining the inhibitory effect of ampicillin loaded into the scaffolds against the common pathogen E. coli. Remarkably, all the scaffolds demonstrated a clear inhibition zone against E. coli bacterial strains. Notably, the luffa-based scaffolds, particularly those with 5% and 3% LC, exhibited a larger zone of inhibition i.e. 13

mm and 10 mm from the external boundaries of the scaffolds to the control scaffold (without luffa) and positive control (ampicillin-loaded Whatman filter paper) when combating the pathogens (Figure 3.9). The study suggests that a controlled release of antibiotics can significantly enhance their inhibitory potential against bacterial strains by ensuring consistent and localized delivery of therapeutic agents. In contrast, the positive control and control scaffolds (without luffa) displayed smaller inhibition zones 8 mm and 9 mm against E.coli; indicating that the higher porosity in these scaffolds led to a faster drug release, resulting in a reduced inhibitory effect. As indicated by our previous analysis of porosity (Gundu et al. 2022), the control scaffold exhibited higher porosity than the 3% LC and 5% LC scaffolds. This difference in porosity likely allowed for a controlled and sustained release of the drug in the 5% LC scaffold, contributing to its larger zone of inhibition compared to the 3% LC, control, and positive control scaffolds. Luffa-based scaffolds often have a porous structure that provides a favorable environment for the gradual release of antimicrobial compounds. The pores within the scaffold can act as reservoirs for the antimicrobial agents; enabling a sustained release over time.

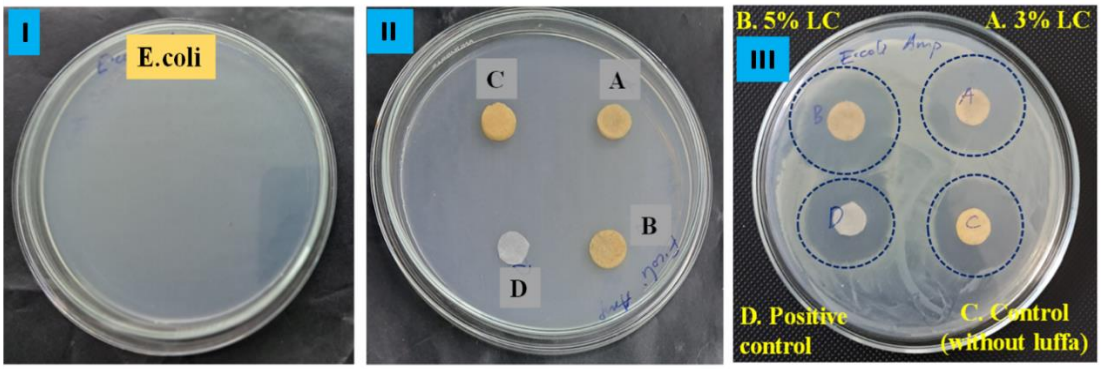

Figure 3.9: Depicts the antibacterial drug release test (I) represents the control Petri plate with E. coli bacterial colony spread. (II) Placement of antibacterial drug-loaded scaffolds and (III) zone of clearance after 24 h.

The biomaterial scaffolds can retain the drug more effectively than filter paper, which may cause the sustained release of the antimicrobial agent over time. The sustained release contributes to a prolonged inhibition effect and a larger inhibition zone. Filter paper lacks such

a drug delivery mechanism, resulting in rapid diffusion of the drug over a larger area. This faster drug release from the filter paper leads to a smaller inhibition zone.

3.5 Conclusion

The results of the investigation revealed that all rats in the experimental groups successfully underwent subcutaneous implantation surgery and had no complications during the three-week postoperative period. The scaffolds used were also found to be biocompatible, as they facilitated cell invasion without causing any inflammatory response. Additionally, there were no signs of implant rejection in any of the rats throughout the experiment; indicating that the luffa-based scaffolds were successfully integrated. All group's histological analyses showed no inflammation or toxicity in animal models; indicating a favorable implanted scaffold response. A 24 h period showed increased levels of AST, ALT, ALP, bilirubin, CK-MB, and serum creatinine. Following implantation, these values recovered to normal within 3 weeks. Notably, luffa-based scaffolds did not significantly raise these parameters compared to control groups; indicating no deleterious effects on the heart, liver and kidney. In conclusion, we have successfully established an implantable scaffold, which satisfied the basic criterion of tissue engineering applications, and provided a concept for regeneration medicine. The outcomes of this study provide highly promising results; demonstrating the excellent in vivo biocompatibility of the luffa-based composite scaffolds. The successful integration of the scaffolds, absence of inflammatory responses, and overall tissue compatibility underscore the significant potential of these scaffolds in diverse tissue engineering and regenerative medicine applications.

3.6 References

Afewerki, Samson, Amir Sheikhi, Soundarapandian Kannan, Samad Ahadian, and Ali Khademhosseini. 2019. "Gelatin-Polysaccharide Composite Scaffolds for 3D Cell Culture and Tissue Engineering: Towards Natural Therapeutics." *Bioengineering & Translational Medicine* 4 (1): 96–115. https://doi.org/10.1002/btm2.10124.

Cabaniss, C. Daniel. 1990. "Creatine Kinase." In *Clinical Methods: The History, Physical, and Laboratory Examinations*, edited by H. Kenneth Walker, W. Dallas Hall, and J. Willis Hurst, 3rd ed. Boston: Butterworths. http://www.ncbi.nlm.nih.gov/books/NBK352/.

Chinnappan, Raja, Tanveer Ahmad Mir, Sulaiman Alsalameh, Tariq Makhzoum, Salma Adeeb, Khaled Al-Kattan, and Ahmed Yaqinuddin. 2023. "Aptasensors Are Conjectured as Promising ALT and AST Diagnostic Tools for the Early Diagnosis of Acute Liver Injury." *Life* 13 (6): 1273. https://doi.org/10.3390/life13061273.

Delanaye, Pierre, Etienne Cavalier, and Hans Pottel. 2017. "Serum Creatinine: Not So Simple!" *Nephron* 136 (4): 302–8. https://doi.org/10.1159/000469669.

Divakar, Prajan, Karen L Moodie, Eugene Demidenko, P Jack Hoopes, and Ulrike G K Wegst. 2020. "Quantitative Evaluation of the *in Vivo* Biocompatibility and Performance of Freeze-Cast Tissue Scaffolds." *Biomedical Materials* 15 (5): 055003. https://doi.org/10.1088/1748-605X/ab316a.

G Srikanth et al. 2009. "Establishment of a Rat Model of Myocardial Infarction with a High Survival Rate: A Suitable Model for Evaluation of Efficacy of Stem Cell Therapy." *Journal of Stem Cells and Regenerative Medicine* 5 (1): 30–36. https://doi.org/10.46582/jsrm.0501006.

Gundu, Shravanya, Ajay Kumar Sahi, Neelima Varshney, Johny Varghese, Niraj K. Vishwakarma, and Sanjeev Kumar Mahto. 2022. "Fabrication and in Vitro

Characterization of Luffa-Based Composite Scaffolds Incorporated with Gelatin, Hydroxyapatite and Psyllium Husk for Bone Tissue Engineering." *Journal of Biomaterials Science, Polymer Edition* 33 (17): 2220–48. https://doi.org/10.1080/09205063.2022.2101415.

Hasan, Kazi Md. Mahmudul, Nasrin Tamanna, and Md. Anwarul Haque. 2018. "Biochemical and Histopathological Profiling of Wistar Rat Treated with Brassica Napus as a Supplementary Feed." *Food Science and Human Wellness* 7 (1): 77–82. https://doi.org/10.1016/j.fshw.2017.12.002.

Hosseinkhani, Mohsen, Davood Mehrabani, Mohammad Hassan Karimfar, Salar Bakhtiyari, Amir Manafi, and Reza Shirazi. 2014. "Tissue Engineered Scaffolds in Regenerative Medicine." *World Journal of Plastic Surgery* 3 (1): 3–7.

Ikada, Yoshito. 2006. "Challenges in Tissue Engineering." *Journal of The Royal Society Interface* 3 (10): 589–601. https://doi.org/10.1098/rsif.2006.0124.

Khorramirouz, Reza, Jason L. Go, Christopher Noble, Soumen Jana, Eva Maxson, Amir Lerman, and Melissa D. Young. 2018. "A Novel Surgical Technique for a Rat Subcutaneous Implantation of a Tissue Engineered Scaffold." *Acta Histochemica* 120 (3): 282–91. https://doi.org/10.1016/j.acthis.2018.02.010.

Kim, Ah Young, Yongsun Kim, Seung Hoon Lee, Yongseok Yoon, Wan-Hee Kim, and Oh-Kyeong Kweon. 2017. "Effect of Gelatin on Osteogenic Cell Sheet Formation Using Canine Adipose-Derived Mesenchymal Stem Cells." *Cell Transplantation* 26 (1): 115–23. https://doi.org/10.3727/096368916X693338.

Kim, Hae, and Mi Han. 2018. "Association between Serum Liver Enzymes and Metabolic Syndrome in Korean Adults." *International Journal of Environmental Research and Public Health* 15 (8): 1658. https://doi.org/10.3390/ijerph15081658.

Kurapati, Rahul, and Michael P. Soos. 2023. “CPK-MB.” In *StatPearls*. Treasure Island (FL): StatPearls Publishing. http://www.ncbi.nlm.nih.gov/books/NBK557591/.

Liu, Runheng, Yixiong Lin, Jinying Lin, Linjun Zhang, Xueli Mao, Baoxin Huang, Yin Xiao, Zhuofan Chen, and Zetao Chen. 2018. “Blood Prefabrication Subcutaneous Small Animal Model for the Evaluation of Bone Substitute Materials.” *ACS Biomaterials Science & Engineering* 4 (7): 2516–27. https://doi.org/10.1021/acsbiomaterials.8b00323.

Mao, Angelo S., and David J. Mooney. 2015. “Regenerative Medicine: Current Therapies and Future Directions.” *Proceedings of the National Academy of Sciences* 112 (47): 14452–59. https://doi.org/10.1073/pnas.1508520112.

Modulevsky, Daniel J., Charles M. Cuerrier, and Andrew E. Pelling. 2016. “Biocompatibility of Subcutaneously Implanted Plant-Derived Cellulose Biomaterials.” *PLOS ONE* 11 (6): e0157894. https://doi.org/10.1371/journal.pone.0157894.

Mohapatra, Bijayinee, and Tapash R Rautray. 2021. “Facile Fabrication of *Luffa Cylindrica* - Assisted 3D Hydroxyapatite Scaffolds.” *Bioinspired, Biomimetic and Nanobiomaterials* 10 (2): 37–44. https://doi.org/10.1680/jbibn.20.00011.

Natsukawa, Tomoaki, Norikazu Maeda, Shiro Fukuda, Masaya Yamaoka, Yuya Fujishima, Hirofumi Nagao, Fumi Sato, et al. 2017. “Significant Association of Serum Adiponectin and Creatine Kinase-MB Levels in ST-Segment Elevation Myocardial Infarction.” *Journal of Atherosclerosis and Thrombosis* 24 (8): 793–803. https://doi.org/10.5551/jat.38232.

Ota, Takayo, Yoshikazu Hasegawa, Eriko Murata, Noriko Tanaka, and Masahiro Fukuoka. 2020. “False-Positive Elevation of CK-MB Levels with Chest Pain in Lung

Adenocarcinoma." *Case Reports in Oncology* 13 (1): 100–104. https://doi.org/10.1159/000505724.

Patamia, Vincenzo, Roberto Fiorenza, Ilaria Brullo, Massimo Zambito Marsala, Stefano Andrea Balsamo, Alfio Distefano, Pio Maria Furneri, Vincenzina Barbera, Salvatore Scirè, and Antonio Rescifina. 2022. "A Sustainable Porous Composite Material Based on Loofah-Halloysite for Gas Adsorption and Drug Delivery." *Materials Chemistry Frontiers* 6 (16): 2233–43. https://doi.org/10.1039/ D2QM00505K.

Thammitiyagodage, M. G., N. R. De Silva, C. Rathnayake, R. Karunakaran, Kumara Wgss, M. M. Gunatillka, N. Ekanayaka, B. P. Galhena, and M. I. Thabrew. 2020. "Biochemical and Histopathological Changes in Wistar Rats after Consumption of Boiled and Un-Boiled Water from High and Low Disease Prevalent Areas for Chronic Kidney Disease of Unknown Etiology (CKDu) in North Central Province (NCP) and Its Comparison with Low Disease Prevalent Colombo, Sri Lanka." *BMC Nephrology* 21 (1): 38. https://doi.org/10.1186/s12882-020-1693-3.

Yilmaz, Ahmet, Kenan Yalta, Okan Onur Turgut, Mehmet Birhan Yilmaz, Ali Ozyol, Omer Kendirlioglu, Filiz Karadas, and Izzet Tandogan. 2006. "Clinical Importance of Elevated CK-MB and Troponin I Levels in Congestive Heart Failure." *Advances in Therapy* 23 (6): 1060–67. https://doi.org/10.1007/ BF02850226.

Zawidlak-Węgrzyńska, Barbara, Miroslawa El Fray, Karolina Janiczak, Roman Kustosz, Małgorzata Gonsior, and Beniamin Oskar Grabarek. 2022. "In Vivo Biocompatibility of an Innovative Elastomer for Heart Assist Devices." *Polymers* 14 (5): 1002. https://doi.org/10.3390/polym14051002.